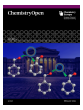

Oxidation of Benzyl Alcohol Using Cobalt Oxide Supported Inside and Outside Hollow Carbon Spheres

Pumza Mente,[a, b] Victor Mashindi,[b] Tumelo N. Phaahlamohlaka,[b] Thabo N. Monyatsi,[b] Roy P. Forbes,[b] and Neil J. Coville*[a, b]

Cobalt oxide nanoparticles (6 nm) supported both inside and outside of hollow carbon spheres (HCSs) were synthesized by using two different polymer templates. The oxidation of benzyl alcohol was used as a model reaction to evaluate the catalysts. PXRD studies indicated that the Co oxidation state varied for the different catalysts due to reduction of the Co by the carbon, and a metal oxidation step prior to the benzyl alcohol oxidation enhanced the catalytic activity. The metal loading influenced the catalytic efficiency, and the activity decreased with increasing metal loading, possibly due to pore filling effects. The catalysts showed similar activity and selectivity (to benzaldehyde) whether placed inside or outside the HCS (63% selectivity at 50% conversion). No poisoning was observed due to product build up in the HCS.

1. Introduction

The catalytic performance and efficiency of a material is evaluated based on its activity, selectivity and stability.[1] Many catalysts are placed on a support to enhance the metal particle surface concentration, and the catalyst support material is thus an important factor that influences catalytic efficiency.[2] Catalyst support materials include titania, alumina, silica, tungsten oxide, and carbon.[3,4] Metal oxide supports have the advantage that they can be used at high temperatures but have the disadvantage of forming strong interactions with metal nanoparticles, leading to reduced catalytic activity via the formation of metal-support compounds, which are not catalytically active.[5] In contrast, carbon supports are relatively chemically inert, and therefore do not form strong metal-to-support interactions.[6] Many carbon based supports that have been used in catalytic reactions include nanofibers, nanotubes, spheres, hollow spheres, nanodiamonds, graphene and carbon black.[7–9] In this study focus will be placed on using hollow carbon spheres (HCSs) as a support and to study the effect of placing a catalyst (Co_xO_y) either inside or outside a HCS.

HCSs have found applications in many fields such as catalysis, gas storage, electrocatalysis, as templates for the synthesis of other hollow spheres, electrode materials for lithium ion batteries and water purification.[10–12] They find use in all these applications because they have unique and desirable structural characteristics that include a high surface area, low density, a mesoporous shell, uniform particle size, narrow pore size distribution and a relatively high oxidation stability.[13–15] The catalytically active materials can be supported either inside and/or outside of the HCSs. By varying the shell porosity, access to/from the HCS interior by reactants/products can be modified. Numerous studies that have been reported in which metals have been placed outside a HCS revealed that the carbon acts as a classical carbon support.[9,16–20] Fewer studies have been reported in which a metal catalyst has been placed inside the HCSs; these studies include reports on Pt, Pd, Cu, Co, Au and alloys as catalysts.[21–28] Comparative studies in which metals have been placed both inside and outside HCSs are rare. In this study we have supported Co oxide nanoparticles both inside and outside HCSs and wish to compare their different catalytic activities/selectivities.

The catalytic oxidation of benzyl alcohol to benzaldehyde was used in this study as a model reaction to evaluate these new Co catalysts. The oxidation of alcohols to the corresponding carbonyl compounds (aldehyde, ketones, carboxylic acids) has been widely investigated and reported in literature.[20,29] These oxidation reactions produce starting materials for the production of important organic compounds that are used for the synthesis of various industrial and consumer products.[30,31] Benzaldehyde is useful in the production of pharmaceuticals, pesticides, perfumes, dyes and aromatic compounds.[32,33] Different oxidizing agents have been used for the oxidation of benzyl alcohol, including the use of hydrogen peroxide, manganese dioxide, permanganate and dichromate.[34–37] Catalytic oxidation, using air or molecular oxygen in the presence of a heterogeneous catalyst, is a more environmentally friendly approach and this oxidant has also shown good efficiency.[38,39] Many current methods for the oxidation of benzyl alcohol can suffer disadvantages, such as long reaction times and low efficiencies.[33]

[a] P. Mente, Prof. N. J. Coville
DSI-NRF Centre of Excellence in Strong Materials
University of the Witwatersrand
2050 Johannesburg (South Africa)
E-mail: neil.coville@wits.ac.za
[b] P. Mente, Dr. V. Mashindi, Dr. T. N. Phaahlamohlaka, T. N. Monyatsi, Dr. R. P. Forbes, Prof. N. J. Coville
Molecular Sciences institute, School of Chemistry
University of the Witwatersrand
2050 Johannesburg (South Africa)

Supporting information for this article is available on the WWW under https://doi.org/10.1002/open.202000312

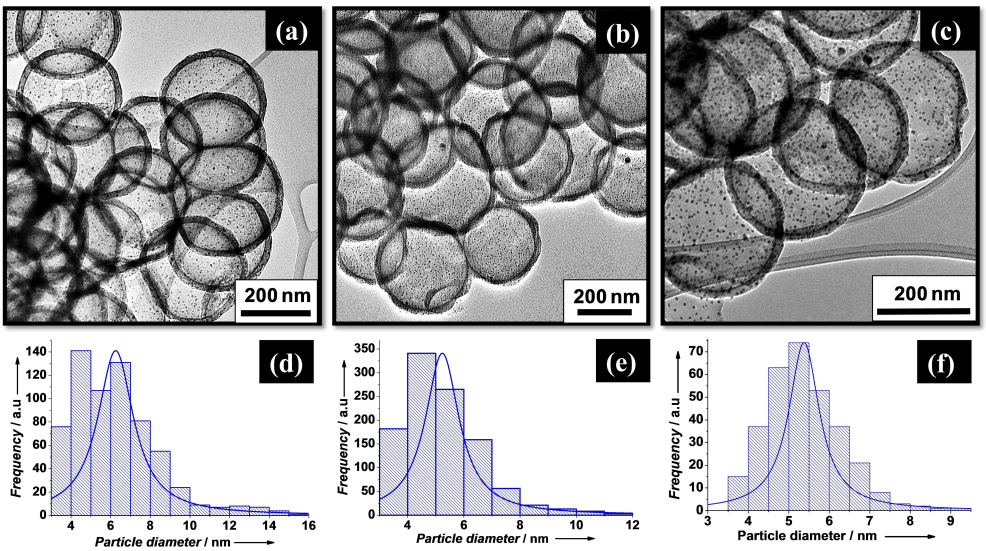

Figure 1. TEM micrographs (a,b,c) and particle size distribution curves (d,e,f) of (a,d) 5%Co_xO_y/HCSs, (b,e) 10%Co_xO_y/HCSs and (c,f) 15%Co_xO_y/HCSs.

Oxidation of simple small-chain alcohols is normally easy and straightforward. However, the oxidation of complex molecules is usually complicated by the production of unwanted carboxylic acid compounds that may cause catalyst deactivation.[39–41] The oxidation of benzyl alcohol to benzaldehyde usually leads to the formation of benzoic acid, benzyl benzoate and toluene as by-products.[29,30] Therefore, the ideal catalyst for this reaction is one that will selectively produce benzaldehyde in large amounts. Noble metal catalysts such as Pt, Pd, Au, Rh, Ir and Ru have been investigated for this process and good activity and selectivity have been achieved.[31,38] However, these metals are expensive and, in some cases, require the use of promoters such as NaOH and K_2CO_3 to control the selectivity during the reaction.[29,42] Non-noble metals like Co, Ni, Fe and Cu are relatively cheaper alternatives that have also been used without the use of promoters and can provide high selectivity.[43] These catalysts, however, suffer from low activity[33,43] and therefore there is still a need for the development of efficient heterogeneous catalysts for the oxidation of benzyl alcohol to benzaldehyde. This can be achieved through manipulation of the material properties by tuning the metal particle size and support material properties such as surface area, porosity and electronic structure. In this study Co oxide nanoparticles were supported either inside or outside HCSs viz. Co_xO_y@HCSs and Co_xO_y/HCSs, respectively. The Co_xO_y@HCSs catalysts were synthesized by using two different types of templates, polystyrene (PS) and the co-polymer, PS-*b*-poly(acrylic acid) containing 12% acrylic acid (PS-*b*-PAA_{12}) and were named Co_xO_y@HCSs_PS and Co_xO_y@HCSs_PS-*b*-PAA_{12}, respectively.[44] Catalysts with different Co loadings, different Co sizes and different Co oxidation states were studied.

2. Results and Discussion

2.1. Catalyst Characterization

Figure 1 shows TEM images and particle size distribution curves for the Co_xO_y nanoparticles supported outside the HCSs (Co_xO_y/HCSs). The nanoparticles are well dispersed on the surface of the HCSs with small particle sizes of 6.2 nm, 5.2 nm and 5.4 nm for the 5%, 10% and 15% metal loaded catalysts, respectively. The synthesis and characterization of Co_xO_y nanoparticles loaded inside the HCSs (5, 10 and 15% Co_xO_y@HCSs) were described previously.[44] The catalyst properties (particle sizes, Co loadings and BET surface area, pore size and pore volumes) are summarized in Table 1. The particle sizes for the Co_xO_y/HCSs are comparable to the values reported for the Co_xO_y@HCSs catalysts (Table 1[44]). The measured internal diameters of the Co_xO_y/HCSs were 263, 311 and 271 nm for the 5%, 10% and

Table 1. Summary of catalyst properties (Co diameter, Co loading and BET surface area).

C[a]	TEM d[b]/nm	PXRD d[b]/nm	Co/ %[c]	Co_3O_4/ %[c]	SA[d]/ $m^2 g^{-1}$	PD[e]/ nm	PV[f]/ $cm^3 g^{-1}$
A[g]	6.1	12.7	4.6	6.3	612	4.8	0.57
B[g]	6.1	6.6	4.6	6.3	506	4.7	0.45
C	6.2	6.8	6.0	8.2	540	5.0	0.67
D[g]	38	18.1	12.1	17.0	316	7.0	0.47
E[g]	6.0	>4	11.0	15.0	479	5.0	0.46
F	5.2	7.5	9.5	12.9	530	4.7	0.63
G[g]	44	18.7	16.4	22.5	388	5.1	0.41
H[h]	5.6	>4	14.3	19.6	536	4.5	0.43
I	5.4	6.3	13.0	17.5	498	5.2	0.51

[a] Catalysts A) 5%Co_xO_y@HCSs_PS, B) 5%Co_xO_y@HCSs_PS-*b*-PAA_{12}, C) 5% Co_xO_y/HCSs, D) 10%Co_xO_y@HCSs_PS, E) 10%Co_xO_y@HCSs_PS-*b*-PAA_{12}, F) 10%Co_xO_y/HCSs, G) 15%Co_xO_y@HCSs_PS, H)15%Co@HCSs_ PS-*b*-PAA_{12} and I)15%Co/HCSs. [b] Particle diameter. [c] Determined by TGA. [d] BET surface area. [e] Pore diameter. [f] Pore volume. [g] Data taken from reference [44]. [h] Characterizations for this catalyst are contained in supplementary Figures S1–S3 in the Supporting Information.

15% catalysts, respectively. The HCS shell thicknesses were found to be 19, 23 and 19 nm for the 5%, 10% and 15% catalysts, respectively. These internal diameters and shell thickness are comparable to the values observed for the metal loaded Co_xO_y@HCSs catalysts.[44] The similarities in these properties allows for a comparison of the effect of the Co location on the benzyl alcohol oxidation reaction.

The PXRD patterns of the Co_xO_y/HCSs catalysts are reported in Figure 2. The broad peaks observed between ~8.4° and ~14°

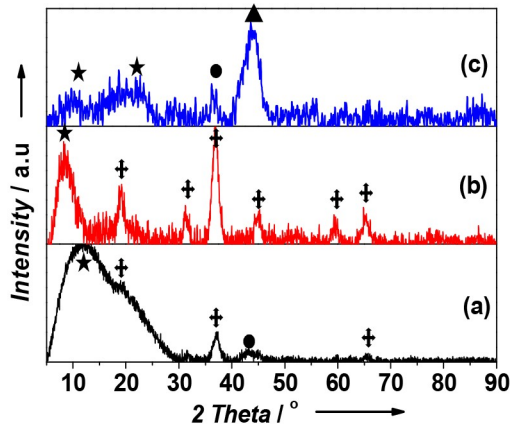

Figure 2. PXRD patterns of (a) 5%Co_xO_y/HCSs, (b) 10%Co_xO_y/HCSs and (c) 15%Co_xO_y/HCSs.

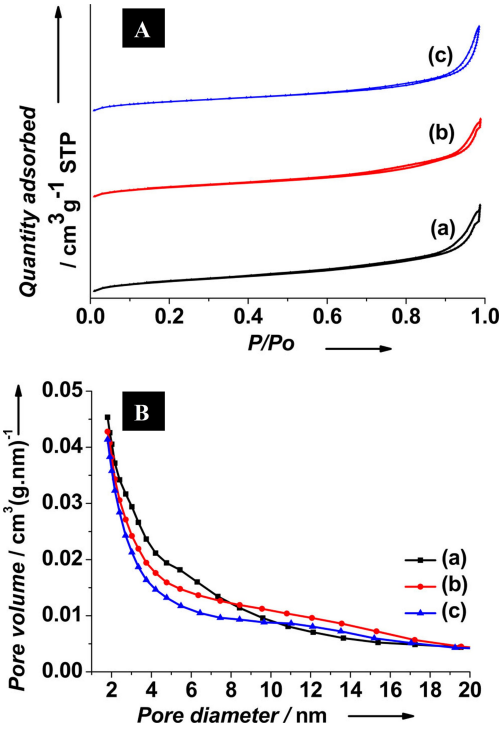

Figure 3. BET isotherms (A) and pore size distribution curves (B) of (a) 5% Co_xO_y/HCSs, (b) 10%Co_xO_y/HCSs and (c) 15%Co_xO_y/HCSs.

for the 5%, 10% and 15% catalysts, are due to the presence of amorphous carbon.[45] The Co crystallite sizes were calculated using the Scherrer equation by integrating the main Co_xO_y peak in the corresponding PXRD diffractograms (Figure 2) are reported in Table 1. The calculated crystallite sizes were 6.8 nm, 7.5 nm and 6.3 nm for the 5%, 10% and 15% catalysts, respectively.

The amorphous carbon was expected as it has been previously observed with carbon prepared from resorcinol-formaldehyde.[46] The spectra show the presence of mainly Co_3O_4 for the 5% and 10% catalysts. However, the PXRD of the 5% catalyst also indicates the possible presence of a small amount of CoO. The 15% catalyst contained mainly fcc Co and CoO. The PXRD peak positions are summarized on Tables S1, S2 and S3. The PXRD patterns of the Co_xO_y@HCSs were previously reported and also showed the presence of a mixture of Co_3O_4, CoO and Co nanoparticles (Tables S1–S3 in the Supporting Information).[44] It is clear that the reduction of the Co was affected by the Co loading (see below).

Figure 3 shows the BET isotherms (A) and pore size distribution curves (B) of the Co_xO_y/HCSs catalysts. The adsorption-desorption curves are characteristic of a combination of type IV and type I isotherms, which indicate the presence of mesopores and some micropores.[47] The pore size distribution curves further confirm the presence of micropores and mesopores, as shown by the high volume of pores with diameters less than 2 nm.

The BET surface areas, pore volumes and pore diameters of all catalysts are reported on Table 1. The surface areas of the 5%, 10% and 15%Co_xO/HCSs catalysts were 540, 530 and 498 $m^2 g^{-1}$, respectively. Similar pore diameters (5.0, 4.7 and 5.2 nm) and pore volumes (0.67, 0.63 and 0.51 $m^3 g^{-1}$) were reported for the 5%, 10% and 15%Co_xO/HCSs catalysts, respectively. The N_2 adsorption-desorption properties of the Co_xO_y/HCSs were comparable to the properties reported for the Co_xO_y@HCSs catalysts (Table 1[44]).

The TGA and derivative TGA curves of the Co_xO/HCSs catalysts are reported in Figure 4. The TGA curves (4A) were used to estimate the content of Co_3O_4 present in the catalysts. The Co_3O_4 contents were 8.2, 12.9 and 17.5% for the 5, 10 and 15% Co_xO/HCSs catalysts, respectively (Table 1) and thus the corresponding Co metal contents (6.0, 9.5 and 13.0%) were close to the loadings used in the synthesis. The estimated metal loadings of all the catalysts are reported in Table 1, and the expected trends can be seen for 5%, 10% and 15% catalysts.

An oxidation peak (blue circle, Figure 4) can be observed for the 15% catalyst at ~240 °C (onset = 190 °C) indicating oxidation of Co to CoO and Co_3O_4. The result is expected as the PXRD of the 15% catalyst indicated the presence of mainly Co.

The derivative TGA curves (4B) show a relatively higher decomposition temperature for the 5% catalyst relative to the 10% and 15% catalysts. This was expected as the carbon decomposition temperature is influenced by the presence of metal nanoparticles. Deconvoluted curves indicated the presence of possibly 3 decomposition maxima for the 5% (326, 363 and 414 °C), 10% (288, 314 and 344 °C) and 15% (284, 337 and 413 °C) Co_xO/HCSs catalysts. The position and breadth of the

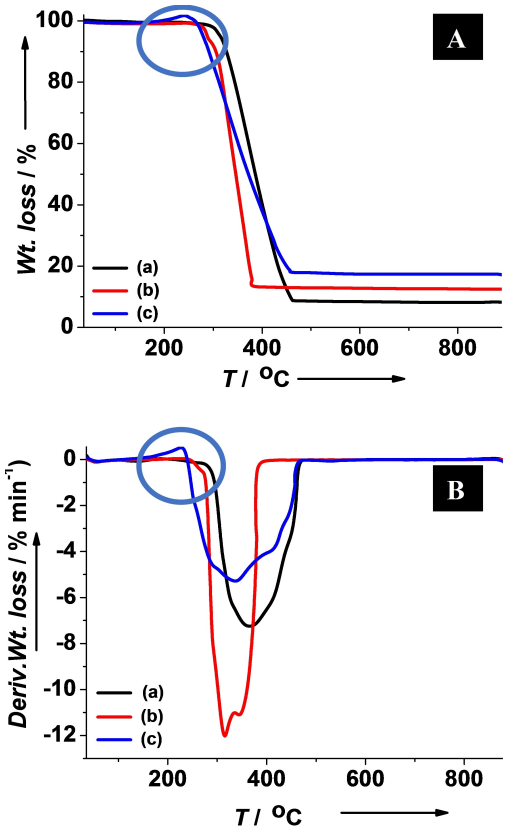

Figure 4. TGA (A) and derivative TGA curves (B) of (a) 5%Co_xO_y/HCSs, (b) 10%Co_xO_y/HCSs and (c) 15%Co_xO_y/HCSs.

peaks is due to the catalytic effect of the oxidation of the HCS carbon by Co. The higher loading of Co led to the peaks for the 10% and 15% loaded catalysts being observed at lower oxidation temperatures than for the 5% loaded HCSs. Importantly, all the catalysts showed comparable thermal stability and they were all stable at the temperature (110 °C) used in the catalytic oxidation reactions.

2.2. Catalyst Activity: Oxidation of Benzyl Alcohol

The new materials were studied as catalysts by using a model reaction: the conversion of benzyl alcohol into benzaldehyde using molecular oxygen as the oxidant. The same amount of reactants, solvents and the same gas flow rates were used in all reactions. The activity was investigated by comparing metal loading as well as the effect of supporting the metal nanoparticles inside or outside HCSs at similar Co loadings. The catalysts were also calcined at 200 °C for 2 h (4 h for the 15% loaded catalysts) in 5%O_2/He and the catalytic activity before and after calcination was recorded. This was required since the Co was heated to 600 °C under an inert atmosphere to polymerize the RF and at these temperatures the carbon can reduce the Co (see below). Furthermore, the use of a PAA functionalized template in the synthesis of the Co_xO_y@HCSs catalysts resulted in different Co oxidation states. The activity data for the calcined catalysts are given in Figures 5 and 6, and the data is summarized on Table 2. The data relates to the

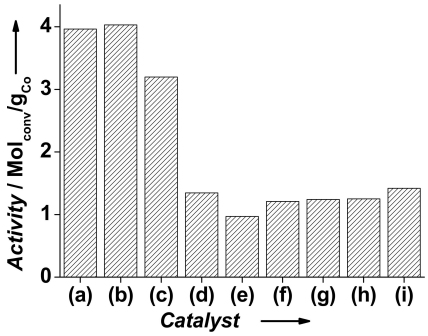

Figure 5. Catalytic activity of the calcined catalysts as mols of benzyl alcohol converted per gram of Co($mols_{conv}/g_{Co}$) for catalysts (a) 5%Co_xO_y@HCSs_PS, (b) 5%Co_xO_y@HCSs_PS-b-PAA12, (c) 5%Co_xO_y/HCSs, (d) 10%Co_xO_y@HCSs_PS, (e) 10%Co_xO_y@HCSs_PS-b-PAA12, (f) 10%Co_xO_y/HCSs, (g) 15%Co_xO_y@HCSs_PS, (h) 15%Co_xO_y@HCSs_PS-b-PAA12 and (i) 15%Co_xO_y/HCSs.

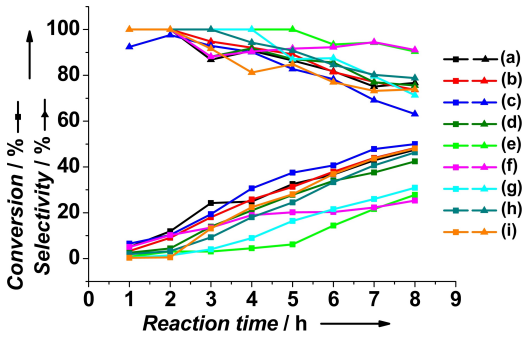

Figure 6. Conversion of benzyl alcohol and selectivity towards benzaldehyde over the calcined catalysts (a) 5%Co_xO_y@HCSs_PS, (b) 5%Co_xO_y@HCSs_PS-b-PAA12, (c) 5%Co_xO_y/HCSs, (d) 10%Co_xO_y@HCSs_PS, (e) 10%Co_xO_y@HCSs_PS-b-PAA12, (f) 10%Co_xO_y/HCSs, (g) 15%Co_xO_y@HCSs_PS, (h) 15%Co_xO_y@HCSs_PS-b-PAA12 and (i) 15%Co_xO_y/HCSs.

Table 2. Conversion, selectivity and catalyst activity of all the catalysts after 8 h of reaction.

Catalyst	BALc Conv.[b]	BALd Select.[c]	Activity/ $mol_{conv}\,g^{-1}{}_{Co}$
5%Co_xO_y@HCSs_PS	35.8	86.1	2.99
5%Co_xO_y@HCSs_PS-b-PAA_{12}	5.2	100	0.43
5%Co_xO_y/HCSs	40.8	82.0	2.61
[a]C-5%Co_xO_y@HCSs_PS	47.5	76.7	3.96
[a]C-5%Co_xO_y@HCSs_PS-b-PAA_{12}	48.3	73.7	4.03
[a]C-5%Co_xO_y/HCSs	50.0	63.1	3.20
10%Co_xO_y@HCSs_PS	41.5	78.2	1.31
10%Co_xO_y@HCSs_PS-b-PAA_{12}	2.5	100	0.09
10%Co_xO_y/HCSs	29.9	87.0	1.21
[a]C-10%Co_xO_y@HCSs_PS	42.4	75.6	1.34
[a]C-10%Co_xO_y@HCSs_PS-b-PAA_{12}	27.8	90.4	0.97
[a]C-10%Co_xO_y/HCSs	25.3	91.1	1.02
15%Co_xO_y@HCSs_PS	53.0	61.3	1.24
15%Co_xO_y@HCSs_PS-b-PAA_{12}	2.8	100	0.05
15%Co_xO_y/HCSs	1.1	100	0.03
[a]C-15%Co_xO_y@HCSs_PS	30.9	71.3	0.72
[a]C-15%Co_xO_y@HCSs_PS-b-PAA_{12}	46.3	78.8	1.25
[a]C-15%Co_xO_y/HCSs	48.1	73.9	1.42

[a] Catalysts calcined at 200 °C for 2 h in 5%O_2/He. [b] Benzyl alcohol conversion. [c] Benzaldehyde selectivity.

activity at 110 °C after 8 h, at atmospheric pressure for reactions performed after catalyst calcination. The data allowed for an exploration of the factors responsible for the variation in catalyst activity.

2.2.1. Effect of Cobalt Oxidation State

Since the catalysts had Co with different oxidation states (see PXRD data in Figure 2 and Tables S1, S2 and S3[44]), the catalysts were also all calcined at 200 °C for 2 h (or 4 h). The calcination was performed at a low temperature to ensure that there was no catalytic conversion of the HCSs to CO_2 in the presence of air (see TGA, Figure 3). As expected, this resulted in improved catalyst activity for most of the catalysts (Table 2). This arises since Co_3O_4 is the required form of the catalysts for the oxidation reaction. In a study by Cordoba and co-workers[31] it was observed (after determining Co^{3+}/Co^{2+} ratios using XPS) that an activation period was required for the catalysts to convert from Co^{2+} to Co^{3+} in the oxidation of benzyl alcohol. They further reported that Co^{3+} was responsible for the catalytic activity while the Co^{2+} was non-active and therefore required activation. In another study by Xie et al.[48] it was reported that both Co^{2+} and Co^{3+} were responsible for the catalytic CO oxidation to CO_2. They reported a mechanism based on theoretical studies, showing that CO molecules adsorb on the Co^{2+} sites, and CO_2 forms by reaction of CO with an O-atom from the Co^{3+} sites. Therefore, the Co^{2+} was responsible for the surface adsorption of CO, while Co^{3+} provided O-atoms. The presence of Co_3O_4 is therefore responsible for catalytic efficiency of cobalt-based catalysts as it contains both Co^{2+} and Co^{3+} sites.

The Co oxidation state varied with the type of support used.

i) The conversion for the 5%Co_xO_y/HCSs catalyst increased from 40.8% to 50% after calcination while the 10%Co_xO_y/HCSs decreased marginally from 29.9% to 25.3% (Table 2). Both these catalysts thus showed small changes with calcination consistent with a dominance of Co_3O_4 in the uncalcined catalysts (Figure 2, Tables S1 and S2 in the Supporting Information). This is expected. However, the 15% Co_xO_y/HCSs catalyst showed a large improvement in conversion after calcination (1.1% to 48.1%) and was consistent with the presence of Co metal in the sample (as seen in the PXRD spectrum in Figure 2) prior to calcination.

The TEM images and particle size distributions of the 5% and 10%Co_xO_y/HCSs after 8 h of benzyl alcohol oxidation were recorded (Figure S8) and the particle diameters are summarized on Table S4. The TEM data showed no clear evidence of any catalyst sintering after reaction. The measured particle diameters were 5.2 nm for both catalysts and the initial diameters were 6.2 and 5.2 nm, for the 5% and 10% catalysts, respectively.

ii) The PXRD data for the 5%Co_xO_y@HCSs_PS indicated that the catalyst prior to calcination consisted mainly of Co_3O_4[44] and thus showed limited improvement after calcination (35.8% to 47.5%, Table 2). Initial analysis of the 10% and 15% Co_xO_y@HCSs_PS catalysts however showed that they consisted mainly of fcc and hcp Co and CoO (Table S2[44]) due to the reduction of Co by carbon, and that the particle had sintered in the synthesis reaction. Oxidation to Co_xO_y readily occurred, and these catalysts showed unexpected high conversions and the conversion only increased marginally (41.5% to 42.4%) for the 10% catalyst after calcination, and even decreased for the 15% catalyst (53% to 30.9%) after calcination.

The TEM images of the 5%, 10% and 15%Co_xO_y@HCSs_PS catalysts after 24 h of reaction are reported in Figure S4 and the particle diameters are summarized in Table S4 in the Supporting Information. There is no observable evidence of further particle sintering in the TEM images taken after 24 h catalytic reaction. The average particle diameters measured from the TEM images are 5.3 nm, 40 nm and 42 nm compared to the initial diameters of 6.1, 38 and 44 nm for the 5%, 10% and 15% catalysts, respectively. The TEM images of the 15%Co_xO_y@HCSs_PS catalyst after the catalytic oxidation reaction showed formation of small hollow spheres within the HCSs (Figures S4 and S5 in the Supporting Information) and the diameter of these small hollow particles was determined to be 45 nm (Table S4 in the Supporting Information). The observation relates to the change in morphology of large Co and Co_xO_y particles as they interconvert.[49] The oxidation of supported metal Co nanoparticles to generate hollow CoOx particles (the Kirkendall effect) is well known in Co catalysed reactions.[49,50] It is presumed that this new morphology is related to the decreased activity.

iii) Large changes in activity occurred for the PS-*b*-PAA_{12} catalysts after calcination. Here, the conversion improved from 5.2% and 2.5% to conversions of 48.3% and 27.8% after calcination, for the 5 and 10% Co loaded catalysts, respectively. The PXRD data (Figure S7) indicated that most of the Co and CoO initially seen in the uncalcined catalyst, was converted to Co_3O_4 species after calcination but even here some fcc Co was still present. A longer calcination time or higher calcination temperature may be required for the 10%Co_xO_y@HCSs_PS-*b*-PAA_{12} catalyst to convert all Co to Co_3O_4 to improve the catalytic activity even further. The 15% catalyst was calcined for 4 h and an improved conversion was also observed (from 2.8% to 46.3%), consistent with the high metal loading in this catalyst. The TEM images and particle size distributions of the reacted 5%, 10% and 15% PS-*b*-PAA_{12} catalysts after 24 h of reaction can be found in Figure S6 and the particle diameters are summarized in Table S4. The measured particles diameters were 5.0 nm, 5.2 nm and 8.9 nm for the 5%, 10% and 15% catalysts, respectively. The initial particles diameters were 6.1 nm, 6.0 nm and 5.6 nm, therefore there is no observed growth for the 5% and 10% catalysts. However, the 15% catalysts showed modest growth after 24 h of reaction.

The Co oxidation state therefore played the key role in the reaction, consistent with known studies.[31,48,51] The results reflect differences in the composition of the catalysts with regards to the quantity of Co, Co^{2+} and Co^{3+} in the initial catalysts. Our studies above confirm the importance of the high oxidation

state required for Co to be used as a catalyst in the benzyl alcohol reaction. No sintering of the Co was observed post reaction even after the calcination steps. Thus, the Co_xO_y reduction by carbon during catalyst synthesis needs to be counteracted by a subsequent calcination process, to convert the Co to Co_3O_4.

2.2.2. Effect of Cobalt Metal Loading

The Co catalyst synthesis procedures used in this study generally gave Co particle sizes between 6–8 nm on both the inside and outside of the HCSs which allowed for a comparative study The effect of metal loading on a per gram basis for the three calcined catalysts is summarized in Figure 4. This shows the data as a function of Co metal loading, with loading determined from the TGA data. The data show that the ($mols_{conv}/g^{-1}_{Co}$) of the three Co catalysts decreased with metal loading from 5% to 10% and then stayed approximately the same from 10% to 15%. In general, the particle sizes from the TEM analysis were between 5–6 nm for most of the catalysts indicating that this was not due to a particle size effect. The exceptions were the 10%Co_xO_y@HCSs_PS and 15% Co_xO_y@HCSs_PS catalysts that had particles larger than 35 nm. Thus, only the effect of metal loading on the Co_xO_y@HCSs_PS-*b*-PAA_{12} and Co_xO_y/HCS catalysts was evaluated in more detail.

i) The conversion for the as synthesized 5% to 15% Co_xO_y@HCSs_PS-*b*-PAA_{12} catalysts increased slowly but at the same rate, i.e. the reactant conversion did not increase with the amount of Co. This could be associated with pore blockage since the surface area/pore volume of the catalysts decreased as the Co content increased (Table 1). After calcination the conversion data for the three catalysts had increased due to conversion of the Co to Co_3O_4, as discussed above.
ii) The Co_xO_y/HCS catalysts, before calcination, gave data that related to the Co oxidation state. After calcination the 5% and 10% catalysts did not show substantial changes while the 15% catalysts did, as discussed above. Again, the key finding is that the activity did not change with Co loading suggesting that under the reaction conditions diffusion control limits the reaction.

The Co2p XPS spectra of the catalysts is reported in Figure S9 and the BE's are summarized in Table S5. The peaks were assigned with reference to the NIST database,[52] as well as other literature studies.[31,53–55] The 15%Co/HCSs catalyst contained Co^{2+}, confirmed by the presence of the $Co2p_{3/2}$ and $Co2p_{1/2}$ and BE's of 780.0 eV and 795.6 eV, respectively. This was further confirmed by the corresponding strong satellite peaks at 785.4 eV and 802.7 eV. These satellite peaks are usually weaker for Co_3O_4, therefore the strong intensity suggests that they are due to CoO and that the sample contained mainly CoO. The surface of metal nanoparticles is prone to surface oxidation, and therefore the oxide phase was observed by XPS. The Co metal observed in the PXRD data arose since this data was recorded soon after the catalyst synthesis, and prior to substantial oxidation of the Co nanoparticles observed by XPS data at a later time. The absence of Co^{3+} in this sample explains the low catalytic activity of this material before calcination (1.1% conversion, Table 2). The XPS spectra of the calcined 15% Co/HCSs catalyst (Figure S9b) showed the presence of Co_3O_4, indicating that the catalyst was successfully oxidized. The finding was confirmed by the presence of the Co2p3/2 and Co2p1/2 peaks at BE's of 778.0 and 795.3 eV, and the corresponding satellite peaks at 785.0 and 801.6 eV, respectively. A small amount of CoO could still be present, but, due to the complex nature of the XPS spectra of the two Co oxides and the similar BE's of Co and Co_3O_4, a quantitative analysis and assignment of the two oxide phases was not possible. The catalytic activity of this calcined catalyst improved, giving a conversion of 48.1% (Table 2), due to the presence of Co_3O_4.

The corresponding XPS spectra showing the survey, and high resolution O1s, N1s and C1s spectra for the 15%Co/HCSs and calcined Co/HCSs are reported on Figure S10. The atomic percentages of the different elements are summarized in Tables S6 and S7.

2.2.3. Effect of the Co Nanoparticles Placed Inside or Outside the HCSs

Figure 6 shows the conversion and selectivity plots of the calcined catalysts and the following can be observed:

i) At 5% catalyst loading the reaction rates for the calcined catalysts are seen to be similar for all three catalysts, As the Co particle sizes are all about 6 nm this implies that Co placed either inside or outside the HCSs gave the same rate data. This implies that under the reaction conditions used, reactant diffusion to the catalyst surface is similar.
ii) The two 10% loaded catalysts with similar particle sizes ((e) 10%Co_xO_y@HCSs_PS-*b*-PAA_{12}, (f) 10%Co_xO_y/HCSs) followed different trends. The 10%Co_xO_y/HCSs catalyst revealed a normal initial reaction but the catalyst deactivated after ca. 4 h. In contrast, the 10%Co_xO_y@HCSs_PS-*b*-PAA_{12} data showed that the catalyst had to overcome an initial barrier before the rate became similar to that for the 10% Co_xO_y@HCSs_PS catalyst. The reasons for this effect are not presently understood.
iii) At 15% loading the Co_xO_y/HCSs and Co_xO_y@HCSs catalyst reactions gave similar final conversion and activity data. Given that these catalysts had similar properties in terms of metal particle size and BET surface areas, it can be deduced that the reaction rates and activity was independent of the location of the metal particles under the reaction conditions.

In summary, it was found that under the reaction conditions used, the placement of the Co on either side of the HCS shell gives very similar activities for the reaction.

2.2.4. Catalyst Selectivity

All the catalysts showed similar selectivity data (Figure 6) and a selectivity to the benzaldehyde (above 70%) that decreased

with time. Thus, the product selectivity did not appear to be affected by whether the Co was placed inside or outside the HCS.

The finding has implications for the use of these catalysts to discriminate between reactants that can enter the HCS and those that are too large. The use of Co_xO_y@HCSs should allow for the preferential oxidation of small reactants and the rates should be the same as observed for oxidation using Co_xO_y/HCSs.

The product reacted further with the catalyst with time and consequently reduced the required product yield by producing secondary products. The common secondary products for this reaction include benzoic acid, toluene, benzene, benzyl ether and benzyl benzoate[56] and these were all observed in the product GC traces, building up with time. These types of secondary products are known to poison the catalyst.[39–41] A GC-FID spectrum is reported on Figure S10 and the trace products can be observed. The products also appear to have the same effect on the Co, in the three different catalysts. The general observation was that the selectivity towards benzaldehyde showed a gradual decrease as the reaction progressed irrespective of the location of the Co. The data are consistent with findings from other studies,[30,48] and suggests that no extra poisoning of the catalyst occurs if secondary products are formed inside the HCS. A comparison of the results from this study have been made with other literature studies on the reaction (Table S10 in the Supporting Information). The range of variable conditions (Co loading/solvent/T etc.) make a comparison with, and between, these studies difficult.

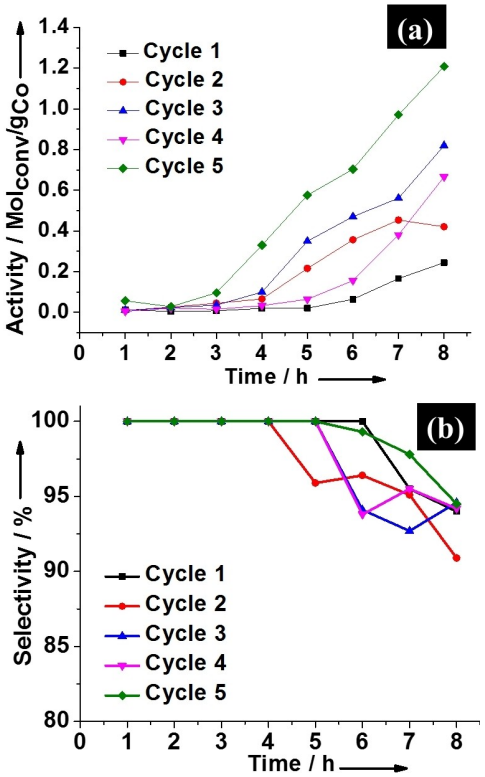

Figure 7. (a) Activity and (b) selectivity towards benzaldehyde during 5 cycles of benzyl alcohol oxidation with 5%Co/HCSs.

2.2.5. Catalyst Recycling

Figure 7 shows the activity and selectivity of the recycled 5% Co/HCS catalyst. Catalyst recycling was achieved by washing the used catalyst with ethanol using magnetic stirring followed by vacuum filtration. The washed catalyst was dried in a 100 °C oven for 4 hours and reused for the oxidation of benzyl alcohol. To ensure minimal losses in mass during the cycles, an initial catalyst mass of 200 mg was used. Losses of approximately 30 mg per cycle occurred. These losses were accurately measured and subtracted when calculating the catalytic activity for each cycle. The catalytic activity showed an increase with recycling and this could be due to the oxidation of the catalyst by oxygen during recycling, therefore making it more active. The by-products which could poison the catalyst were successfully washed off with ethanol. The selectivity is still above 90% even after 5 cycles and indicates that the catalyst is quite stable and re-useable.

The 5%Co@HCSs_PS-b-PAA12 and 10%C0@HCSS_PS-b-PAA12 catalysts could not be recycled. Several methods were used in attempts to regenerate the catalysts and re-activate the active sites. The catalyst was washed several times with DMF, and no benzyl alcohol conversion could be observed. Washing with ethanol also did not give any activity. In another attempt, the washed catalyst was calcined in air at 200 °C for 1 h. This also did not give recovery of the activity. The catalyst was then characterized by TEM, surface analysis and TGA, to understand why there was no activity when attempting to recycle the catalyst. TEM did not show any particle growth, and this was expected as the reaction was done under mild reaction conditions.

Table S8 shows the surface area analysis of the two reacted catalyst. A significant loss in BET surface area occurred for both catalysts. However, the loss was more pronounced for the Co@HCSs catalyst. The Co/HCSs catalyst only lost 50% of the BET SA and the Co@HCSs catalyst lost almost 70%. A significant loss in micropore SA was noted, suggesting a blockage of small pores. The fresh catalyst had a high micropore SA, which was almost 50% of the total SA. It is not understood why the Co/HCSs catalyst had a relatively smaller degree of pore blockage than the Co@HCSs catalyst. The corresponding BET isotherms are reported on Figure S13 in the Supporting Information. The isotherms are typical of a material with type IV pore structures and are an indication of the presence of mesopores. The fresh catalysts contained a combination of Type I and type IV pore structures. The BET isotherms further confirm the possibility of a blockage of the small pores by possible carbon build-up. The pore size distribution curves can be found in Figure S14 in the Supporting Information. It is evident that there is a high volume of pores with ~4 nm diameter. The fresh catalysts contained a high volume of pores less than 2 nm, which are micropores. The catalysts still contain some micropores, in smaller volumes compared to the fresh catalyst. Figure S15 in the Supporting Information shows the TGA and DTGA curves of the recycled

catalyst. An initial weight loss of about 20% can be observed for both catalysts, with an onset at 200 °C. This could be due to the loss of the reaction products that could not be properly washed off from the catalysts. The Co@HCSs catalyst was calcined at 200 °C in an attempt to remove products that could be trapped on the catalyst. However, no recovery of the activity of the catalyst was observed. It is interesting that both catalysts have a similar weight loss at the same temperature, but the Co/HCSs catalyst showed the least loss in BET SA.

3. Conclusion

The Co_xO_y@HCSs and Co_xO_y/HCSs catalysts showed similar activity towards the oxidation of benzyl alcohol (~50% conversion) and produced benzyl alcohol in good yields (> 70%). TEM analysis of the reacted catalysts revealed that all the catalysts showed resistance to metal sintering even after 24 h of reaction. The carbon support was found to reduce the Co_xO_y species and to convert the Co and CoO to Co_3O_4 via calcination to increase the benzyl alcohol conversion. An increase in metal loading led to a decrease in catalyst efficiency and this was seen to be related to a lowered surface area due to pore blockage by the metal. The catalysts inside and outside the HCSs showed very similar activity and selectivity, indicating that the location of the metal on the HCS, under our reaction conditions, was not important for this reaction.

Experimental Section

Materials

Styrene, acrylic acid, polyvinylpyrrolidone (PVP, MW 40 000), resorcinol, formaldehyde solution (37%), cetyltrimethylammonium bromide (CTAB), cobalt nitrate hexahydrate, hydrazine hydrate (78–82%) and benzyl alcohol were all purchased from Sigma Aldrich and used as received. Ammonia solution (25%, Fluka), potassium persulfate (Eimer and Amend), ethanol (98%, MK Labs) and N,N-dimethylformamide (Merck) were also used as received. Distilled water was used for all experiments and washings. Oxygen (technical grade) was purchased from Afrox.

Synthesis of Polymer Spheres (PSs)

Polystyrene spheres (PS) (d = 350 nm) and the co-polymer, polystyrene-*b*-poly (acrylic acid) with 12% PAA (PS-*b*-PAA_{12}) (d = 343 nm) were made as described previously (see[44] and supplementary section).

Synthesis of Co_xO_y Inside HCSs (Co_xO_y @HCSs)

The synthesis of 5% Co_xO_y@HCSs, 10% Co_xO_y@HCSs and 15% Co_xO_y@HCSs were made as described previously using PSSs and PS-*b*-PAA_{12} templates (see[44] and Supplementary section). The synthesis of the corresponding Co_xO_y/PS and resorcinol-formaldehyde (RF) covered Co_xO_y/PS (RF/Co_xO_y/PS) were also made as indicated in.[44]

Synthesis of Co_xO_y Outside HCSs (Co_xO_y/HCSs)

The RF/PS composites were synthesized using the method reported above by making use of PS instead of a Co_xO_y/PS composite. The RF/PS composite (2 g) was dispersed in 50 mL distilled water and 28 mL ethanol by ultrasonication and 0.07 g of cobalt nitrate hexahydrate was added to the mixture while stirring. After 5 minutes (or until all the cobalt salt dissolved), 3.3 mL of 2 M hydrazine hydrate was added slowly (dropwise), and the reaction continued for 12 h, at room temperature. The mixture was filtered by vacuum filtration and the product (CoxOy/RF/PS) was washed with water, dried in the oven at 60 °C for 12 h, crushed with a mortar and pestle and stored in a glass sample vial. The dry product was annealed to produce 5%Co_xO_y/HCSs. Two and three times the amount of cobalt nitrate hexahydrate and hydrazine hydrate were used to synthesize 10%Co_xO_y/HCSs and 15%Co_xO_y/HCSs, respectively.

Catalyst Calcination

The catalysts were calcined by placing ~70 mg of the as-synthesized catalyst in-between two plugs of quartz wool, inside a glass tube reactor. The reactor was placed inside a vertical furnace and heated to 200 °C at a rate of 5 °C/min, under 5%O_2/He flowing at 20 mL/min and kept isothermal for 2 h. Thereafter the catalyst was cooled to room temperature. The 15% metal loaded catalysts were calcined for 4 h to ensure a complete conversion of Co and CoO to Co_3O_4.

Characterization Techniques

TEM analysis was done on a Tecnai Spirit (T12) operating at 120 kV. The samples were dispersed in ethanol by ultrasonication and then loaded on to a lacey carbon copper grid. TEM metal particle sizes were determined using Mipar image analysis software. More than 400 nanoparticles were measured on the TEM images. Thermal analysis was done using a Perkin Elmer TGA 6000 thermogravimetric analyser using high purity nitrogen and air at a heating rate of 10 °C/min and gas flow rate of 10 mL/min. PXRD was performed on a Bruker D2 Phaser with Cu radiation. The PXRD metal particle sizes were determined using Eva diffraction software by applying the Scherrer equation on the most prominent peaks from the corresponding PXRD diffractograms. A Micromeritics Tristar 3000 surface area and porosity analyser operating at −195 °C was used to determine the surface are and porosity of the materials. The samples (100 mg) were degassed at 150 °C for 12 h, under flowing nitrogen. The XPS measurements were carried out using a Thermo Scientific ESCALAB 250Xi spectrometer with a Monochromatic Al Kα source (1486.7 eV) operating with an X-ray power of 300 W, X-ray spot size of 900 μm, low resolution pass energy of 100 eV, high resolution pass energy of 20 eV and a pressure of 10^{-8} mBar.

Catalytic Reactions

Catalyst (50 mg) was added to a 100 mL 3-neck round bottom flask fitted with a reflux condenser, gas inlet and a rubber septa. N,N-dimethylformamide (DMF, 25 mL) and benzyl alcohol (2 mL, 19.2 mmol) were added to the flask and the reaction was heated to 110 °C under 40 mL/min O2 flow and a constant stirring rate. The reaction was continued for 8 h, during which time 0.5 mL aliquots were sampled every hour and analysed by gas chromatography with an FID, using a capillary column (Phenomenex Zebrox, 30 m × 0.53 mm) and N2 as the carrier gas. The products were also analysed with a GC-MS. All the variables were kept constant for the different reactions.

Acknowledgements

This work was supported by the National Research Foundation (NRF), South Africa; the University of the Witwatersrand (Post-graduate Merit Award) and the DSI-NRF Centre of Excellence in Strong Materials (CoE-SM).

Conflict of Interest

The authors declare no conflict of interest.

Keywords: benzaldehyde · alcohol oxidation · cobalt · heterogeneous catalysis · hollow carbon spheres

[1] P. S. Lamoureux, K. T. Winther, J. A. Torres, V. Streibel, Z. Meng, M. Bajdich, F. Abild-Pedersen, T. Bligaard, *ChemCatChem* **2019**, *11*, 3581–3601.
[2] L. J. Garces, B. Hincapie, R. Zerger, S. L. Suib, *J. Phys. Chem. C* **2015**, *119*, 5484–5490.
[3] S. Shama, B. G. Pollet, *J. Power Sources* **2012**, *208*, 96–119.
[4] F. Rodrigues-Reinoso, *Carbon* **1998**, *36*, 159–175.
[5] D. I. Enache, B. Rebours, M. Roy-Auberger, R. Revel, *J. Catal.* **2002**, *205*, 346–353.
[6] K. Cheng, V. Subramanian, A. Carvelho, V. V. Ordomsky, Y. Wang, A. Y. Khodakov, *J. Catal.* **2016**, *337*, 260–271.
[7] N. J. Coville, S. D. Mhlanga, E. N. Nxumalo, A. Shaikjee, *S. Afr. J. Sci.* **2011**, *107*, no. 418.
[8] H. Xiong, M. Moyo, N. K. Rayner, L. L. Jewell, D. G. Billing, N. J. Coville, *ChemCatChem* **2010**, *2*, 514–518.
[9] C. Galeano, J. C. Meier, V. Peinecke, H. Bongard, I. Katsounaros, A. A. Topalov, A. Lu, K. J. Mayrhofer, F. Schuth, *J. Am. Chem. Soc.* **2012**, *134* 20457–20465.
[10] F. Bottger-Hiller, P. Kampe, G. Cox, A. Panchenko, N. Janssen, A. Petzold, T. Thurn-Albrecht, L. Borchardt, M. Rose, S. Kaskel, C. Georgi, H. Lang, S. Spange, *Angew. Chem. Int. Ed.* **2013**, *52*, 6088–6091; *Angew. Chem.* **2013**, *125*, 6204–6207.
[11] S. Ma, P. Su, W. Huang, S. P. Jiang, S. Bai, J. Liu, *ChemCatChem* **2019**, *11*, 6092–6098.
[12] F. Zheng, M. He, Y. Yang, Q. Chen, *Nanoscale* **2015**, *7*, 3410–3417.
[13] S. Li, A. Pasc, V. Feirro, A. Celzard, *J. Mater. Chem. A* **2016**, *4*, 12686–12713.
[14] J. H. Kim, B. Fang, M. Kim, J. Yu, *Catal. Today* **2009**, *146*, 25–30.
[15] J. Qu, H. Zhu, D. Chen, N. Li, Q. Xu, J. Xie, H. Li, H. He, J. Lu, *ChemCatChem* **2018**, *10*, 837–842.
[16] J. Ding, H. Zhang, H. Zhou, J. Feng, X. Zheng, C. Zhong, E. Paek, W. Hu, D. Mitlin, *Adv. Mater.* **2019**, *31*, 1900429.
[17] C. Galeano, J. C. Meier, M. Soorholtz, H. Bongard, C. Baldizzone, K. J. Mayrhofer, F. Schith, *ACS Catal.* **2014**, *4*, 3856–3868.
[18] K. Wenelska, B. Michalkiewicz, J. Gong, T. Tang, R. Kalenczuk, X. Chen, E. Mijowska, *Int. J. Hydrogen Energy* **2013**, *38*, 16179–16184.
[19] K. Ranganathan, A. Morais, I. Nongwe, C. Longo, A. F. Nogueira, N. J. Coville, *J. Mol. Catal. A* **2016**, *422*, 165–174.
[20] V. Ravat, I. Nongwe, R. Meijboom, G. Bepete, N. Coville, *J. Catal.* **2013**, *305*, 36–45.
[21] G.-H. Wang, J. Hilgert, F. H. Richter, F. Wang, H.-J. Bongard, B. Spliethoff, C. Weidenthaler, F. Schuth, *Nat. Mater.* **2014**, *13*, 293–300.
[22] Z. Zhang, F. Xiao, J. Xi, T. Sun, S. Xiao, H. Wang, S. Wang, Y. Liu, *Sci. Rep.* **2015**, *4*, no. 4053.
[23] P. M. Gangatharan, M. S. Maubane-Nkadimeng, N. J. Coville, *Sci. Rep.* **2019**, *9*, no. 10642.
[24] C. Lurhs, J. Philips, M. N. Richard, A. M. Knapp, *United States of America Patent 0215960*, 26 August **2010**.
[25] T. N. Phaahlamohlaka, M. W. Dlamini, D. O. Kumi, R. Forbes, L. L. Jewell, N. J. Coville, *Appl. Catal. A* **2020**, *559*, no. 117617.
[26] C. Zhang, R. Zhang, S. He, L. Li, X. Wang, M. Liu, W. Chen, *ChemCatChem* **2017**, *9*, 980–986.
[27] C. Dong, Q. Yu, P.-P. Ye, P. Su, J. Liu, G.-H. Wang, *Angew. Chem. Int. Ed.* **2020**, *59*, 18374–18379.
[28] Y. Wang, H. Pan, Q. Lin, Y. Shi, J. Zhang, *Catalysts* **2020**, *10*, no. 303.
[29] G. Nagy, A. Beck, G. Safran, Z. Schay, S. Liu, T. Li, B. Qiao, J. Wang, K. Lazar, *React. Kinet. Mech. Catal.* **2019**, *128*, 71–95.
[30] C. Rangupathi, J. J. Vijaya, S. Narayanan, S. K. Jesudoss, L. J. Kennedy, *Ceram. Int.* **2015**, *41*, 2069–2080.
[31] M. Cordoba, C. Miranda, C. Lederhos, F. Coloma-Pascual, A. Ardila, G. A. Fuentes, Y. Pouilloux, A. Ramirez, *Catalysts* **2017**, *7*, no.384.
[32] S. Ji, Y. Chen, Z. Zhang, W.-C. Cheong, Z. Liu, D. Wang, Y. Li, *Nanoscale Horiz.* **2019**, *4*, 902–906.
[33] X. Yang, S. Wu, L. Peng, J. Hu, X. Wang, X. Fu, Q. Huo, J. Guan, *RSC Adv.* **2015**, *5*, 102508–102515.
[34] A. Jia, L.-L. Lou, C. Zhang, Y. Zhang, S. Liu, *J. Mol. Catal. A* **2009**, *306*, 123–129.
[35] V. Ravat, I. Nongwe, N. J. Coville, *ChemCatChem* **2012**, *4*, 1930–1934.
[36] A. Mondal, D. Mukherjee, B. Adhikary, M. A. Ahmed, *J. Nanopart. Res.* **2016**, *18*, no.117.
[37] D. Dey, M. K. Mahanti, *J. Org. Chem.* **1990**, *55*, 5848–5850.
[38] K. Zhang, Y. Lui, J. Deng, L. Jing, W. Pei, Z. Han, X. Zhang, H. Dai, *ChemCatChem* **2019**, *11*, 6398–6407.
[39] J. Zhu, K. Kailasam, A. Fischer, A. Thomas, *ACS Catal.* **2011**, *1*, 342–347.
[40] T. Mallat, A. Baiker, *Chem. Rev.* **2004**, *104*, 3037–3058.
[41] E. Ali, M. Rahman, S. Sarkar, S. B. Hamid, *J. Nanomater.* **2014**, *1*, 1–23.
[42] D. Mao, M. Jia, J. Qiu, X.-F. Zhang, J. Yao, *Catal. Lett.* **2020**, *150*, 74–81.
[43] V. R. Choudhary, P. A. Chaudhari, V. S. Narkhede, *Catal. Commun.* **2003**, *4*, 171–175.
[44] P. Mente, T. N. Phaahlamohlaka, V. Mashindi, N. J. Coville, *J. Mater. Sci.* **2021**, *56*, 2113–2128.
[45] R. Paul, A. A. Voevodin, J. J. Hu, P. B. Amama, S. Ganguli, A. K. Roy, D. Zemlyanov, T. S. Fisher, *Thin Solid Films* **2013**, *528*, 187–193.
[46] L. C. Cotet, M. Gich, A. Roig, I. C. Popescu, V. Cosoveanu, E. Molins, V. Danciu, *J. Non-Cryst. Solids* **2006**, *352*, 2772–2777.
[47] Y. Tao, M. Endo, K. Keneko, *Recent Pat. Chem. Eng.* **2008**, *1*, 192–200.
[48] Y. Xie, F. Dong, S. Heinbuch, J. J. Rocca, E. R. Bernstein, *Phys. Chem. Chem. Phys.* **2010**, *12*, 947–959.
[49] C. J. Weststrate, M. M. Hauman, D. J. Moodley, A. M. Saib, E. van Steen, J. W. Niemantsverdriet, *Top. Catal.* **2011**, *54*, 811–816.
[50] M. Varón, I. Ojea-Jimenez, J. Arbiol, L. Balcells, B. Martínez, V. F. Puntes, *Nanoscale* **2013**, *5*, 2429–2436.
[51] L. Zhong, T. Kropp, W. Baaziz, O. Ersen, D. Teschner, R. Schlogl, M. Mavrikakis, S. Zafeiratos, *ACS Catal.* **2019**, *9*, 8325–8336.
[52] A. V. Naumkin, A. Kraut-Vass, S. W. Gaarenstroom, C. J. Powell, "NIST X-Ray Photoelectron Spectroscopy Database," **2012**. [Online]. Available: srdata.nist.gov/xps/EngElmSrchQuery.aspx?EType=PE&CSOpt=Retri_ex_dat_&Elm=Co. [Accessed 6 February 2021].
[53] M. C. Biesinger, B. P. Payne, A. P. Grosvener, L. M. Lau, A. R. Gerson, R. S. C. Smart, *Appl. Surf. Sci.* **2011**, *257*, 2717–2730.
[54] "Thermo scientific XPS," Thermo Fisher Scientific Inc., [Online]. Available: http://xpssimplified.com/elements/cobalt.php. [Accessed 5 February 2021].
[55] K. Lin, B.-J. Chen, *J. Colloid Interface Sci.* **2017**, *486*, 255–264.
[56] L. Gurrala, A. S. Nagpure, H. R. Gurav, S. Chilukuri, *ChemistrySelect* **2018**, *3*, 3751–3761.

Manuscript received: October 22, 2020
Revised manuscript received: March 29, 2021